ARTICLES

Dynamics Study of the OH + O_2 Branching Atmospheric Reaction. 2. Influence of Reactants Internal Energy in HO_2 and O_3 Formation

P. J. S. B. Caridade, L. Zhang, J. D. Garrido,† and A. J. C. Varandas*,‡

Departamento de Química, Universidade de Coimbra, P-3049 Coimbra, Portugal

Received: November 28, 2000

The effect of reactants vibrational and rotational excitation on products (HO_2 + O and O_3 + H) formation is investigated for the title reaction by using the quasiclassical trajectory method and the realistic double many-body expansion (DMBE) potential energy surface for ground-state HO_3. It is shown that it can be a potential source of ozone in the upper atmosphere.

1. Introduction

The hydrogen−oxygen systems are known to play a key role in atmospheric chemistry,[1−5] with the involved species appearing in both the ground and/or excited states (whenever the electronic term symbols are omitted, the species will be assumed to be in their ground electronic states). For example, the atmospheric reaction

$$H + O_3 \rightarrow OH\,(X^2\Pi, v') + O_2 \qquad (1)$$

leads to OH in vibrationally excited states with vibrational quantum numbers up to $v' = 9$.[6−23] In turn, the photodissociation of ozone within the Hartley band yields vibrationally excited oxygen with a vibrational distribution peaking at both $v'' = 14$ and $v'' = 27$[24] according to the reaction

$$O_3 + h\nu\,(\lambda < 243\ \text{nm}) \rightarrow O_2\,(X^3\Sigma_g^-, v'') + O \qquad (2)$$

There are additional sources of vibrationally excited oxygen molecules in the stratosphere besides eq 2, in particular the reaction

$$O + HO_2 \rightarrow O_2\,(X^3\Sigma_g^-, v'') + OH \qquad (3)$$

where O_2 has been found to populate vibrational states up to $v'' = 13$,[25] and

$$O + O_3 \rightarrow 2O_2\,(X^3\Sigma_g^-, v'') \qquad (4)$$

which can populate levels up to $v'' = 14$.[24,26]

As is well established, ozone plays a crucial role in stratospheric and mesospheric chemistry. Despite this interest, atmospheric models are known to underestimate the measured concentrations of ozone in the upper stratosphere by up to 20%. This 'ozone deficit' problem has prompted much effort to identify new sources of ozone.[27−32] We will show in the present work (see also ref 33, hereafter referred to as paper I), that one possible source may be the reaction

$$OH + O_2 \rightarrow O_3 + H \qquad (5)$$

In fact, the possibility exists that ozone can be formed by selective vibrational excitation of the reactant molecules. Of course, such a reaction can only occur in natural environments where those vibrationally hot species abound, namely in the stratosphere. Note that in the stratospheric ozone layer the pressure is low (about 30 Torr at 25−30 km), and hence relaxation through collisional processes is likely to be slow. As a result, the internal energy distribution of the atmospheric constituents is expected to be far from thermal equilibrium. Thus, the reaction OH(v',j') + O_2(v'',j'') may be a potential source of both HO_2 and O_3, which are vital natural species in atmospheric chemistry. This also implies that it may be necessary to treat the reactants in the various internal states as distinct species in order to obtain good estimates of atmospheric rate coefficients.

In paper I, we have studied the influence of the vibrational excitation of oxygen in formation of hydroperoxyl radical. It was then concluded that, for $v' = 0$, such a product appeared only when $v'' = 13$ over the whole range of translational energies. In turn, ozone was formed only for $v'' = 27$ at translational energies over 20 kcal mol^{-1}, but still with a small reactive cross section. A major goal of the present work is therefore to report a detailed theoretical study of the title branching reaction

$$OH\,(v', j') + O_2\,(v'',j'') \rightarrow HO_2 + O \qquad (6)$$

$$\rightarrow O_3 + H \qquad (7)$$

by considering the excitation of vibrational and rotational degrees of freedom in both molecules. For this, we will employ the quasiclassical trajectory (QCT) method and the realistic single-valued DMBE potential energy surface[34] for the electronic ground state of HO_3, which has been extensively used to study

† Permanent address: Departamento de Física General y Matemática, Instituto Superior de Ciencias y Tecnología Nucleares, 6163 La Havana, Cuba.

‡ E-mail: varandas@qtvs1.qui.uc.pt.

10.1021/jp004308o CCC: $20.00
Published on Web 04/13/2001

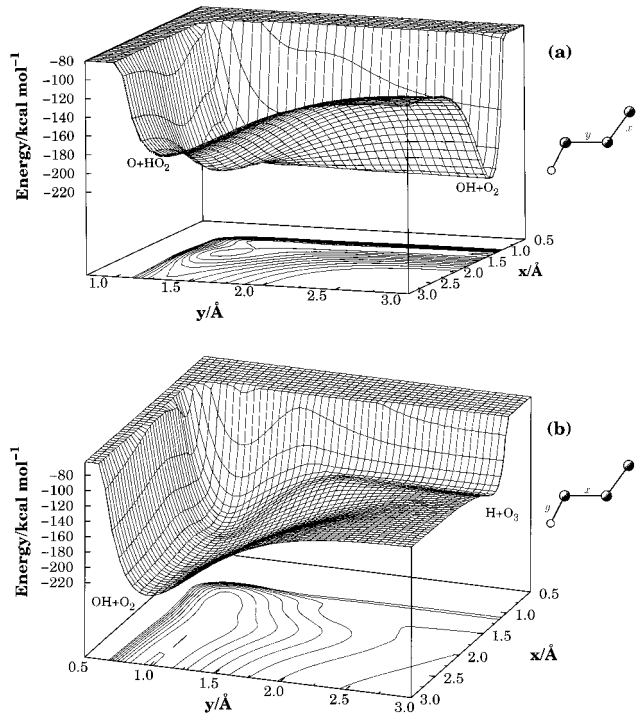

Figure 1. Perspective view of the potential energy surface for the reactions OH(v',j') + O$_2$(v'',j'') → HO$_2$ + O (a) and OH(v',j') + O$_2$(v'',j'') → O$_3$ + H (b).

the reverse of reaction 6[25,35]

$$HO_2 + O \rightarrow OH + O_2 \tag{8}$$

and the reverse of reaction 7[34,36,37]

$$H + O_3 \rightarrow OH + O_2 \tag{9}$$

In both these cases, good agreement with the available experimental data has been obtained. The paper is organized as follows. Section 2 provides a brief survey of the HO$_3$(^{2}A) DMBE potential energy surface, while the computational method is described in section 3. The results are presented and discussed in section 4, while the major conclusions are in section 5.

2. Potential Energy Surface

As in paper I, all calculations reported in this work have employed the six-dimensional (6D) DMBE potential energy surface[34] for the electronic ground state of HO$_3$. Since it has been described in detail elsewhere,[34] we focus here on its main topographical features. Figure 1 shows perspective views of the HO$_3$ potential energy surface for the regions of configurational space with relevance for the reactions studied in the present work. Note that the angles ∠OOO, ∠HOO, and ∠HOOO (torsion), as well as the O−H distance have been partially relaxed ($112.7 \le \theta_{OOO}/\text{deg} \le 118.7$, $94.6 \le \theta_{HOO}/\text{deg} \le 104.3$, $82.6 \le \phi_{HOOO}/\text{deg} \le 90.6$, and $0.9708 \le R_{OH}/\text{Å} \le 1.0315$) when obtaining the plot of Figure 1a. Note especially that this plot differs from the one shown elsewhere,[33] which refers to OH attacking O$_2$ with the H atom pointing toward one of the oxygen atoms. A corresponding relaxation has been considered for Figure 1b, which is more relevant for the analysis of ozone formation: $106 \le \theta_{OOO}/\text{deg} \le 120$, $100 \le \theta_{HOO}/\text{deg} \le 120$, $0 \le \phi_{HOOO}/\text{deg} \le 180$, and $2.26 \le R_{OO}/\text{Å} \le 2.42$.

Figure 2 shows the calculated minimum energy paths for the

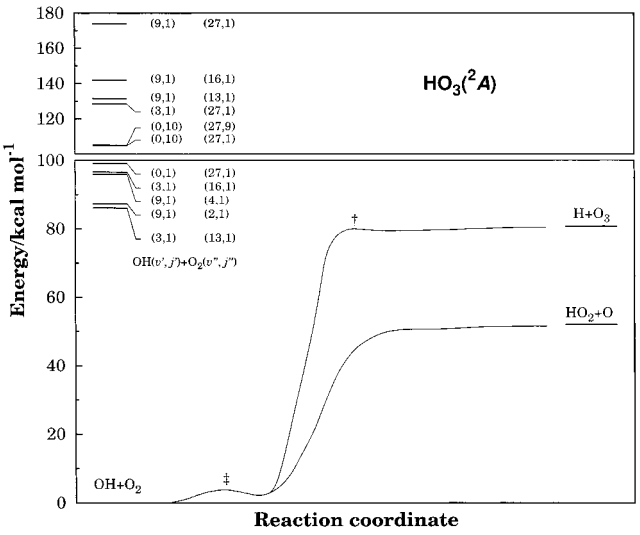

Figure 2. Minimum energy path for formation of HO$_2$ + O and O$_3$ + H. Shown by the symbols † and ‡ are the saddle points for the H + O$_3$ → OH + O$_2$ and HO$_2$ + O → OH + O$_2$ processes, respectively. Also shown are some vibrational energy levels of the two reactant molecules.

reactions 6 and 7. Also shown in this figure is the energetics for various combinations of vibrational and rotational quantum numbers according to the HO$_3$ DMBE potential energy surface. Note that reactions 6 and 7 are feasible over the complete range of translational energies for the internal energy combinations indicated in Figure 2. Ozone formation is found to dominate for highly excited vibrational sates of OH, while HO$_2$ turns out to be the major product for the remaining combinations of internal excitation considered in the present work. The involved trends will be discussed in the results section.

A final remark to note that the current DMBE potential energy surface has been found unable to predict the selectivity of product OH vibrational states reported from experimental work in the case of the reverse H + O$_3$ → OH + O$_2$ reaction.[36] Although this may point out that errors are obviously inherent to the potential energy surface, the uncertainties reported for the experimental vibrational distributions indicate that this is to some extent an issue still open to debate. After this work has been completed, an improved version of the DMBE potential energy surface used in the present work has been obtained (DMBE-II[38]) and used for exploratory studies of the title reaction.[39] Suffice it to say that such results support and even magnify the general trends reported here.

3. Computational Details

Following paper I, the QCT method has been employed as implemented in an extensively adapted version of the MERCURY/VENUS96[40] codes. Calculations have been done for diatom−diatom translation energies over the range $0.1 \le E_{tr}/\text{kcal mol}^{-1} \le 20$; for a summary, see Tables 1−4. However, we have focused the computational effort in the range of small to middle translational energies, which are likely to be of major interest for atmospheric chemistry. Yet, since the batches for low translational energies are computationally expensive, we have limited their number to a minimum judged convenient to get a satisfactory coverage. Working parameters for numerical integration and maximum value of the impact parameter (b_{max}) have been determined as in paper I. Similarly, the initial diatom−diatom separation has been fixed by convenience over the range 8−10 Å, so as to make the interaction negligible.

TABLE 1: Summary of the Trajectory Calculations for OH(v',j'=1) + O_2(v'',j''=1) → HO_2 + O

v'	v''	$E_{vib/rot}$, kcal mol^{-1}	E_{tr}, kcal mol^{-1}	b_{max}, Å	σ^{HO_2}, Å^2	$\Delta\sigma^{HO_2}$, Å^2
3	13	86.075	0.5	5.3	2.303	0.630
			1.0	4.2	1.446	0.395
			2.5	3.0	1.413	0.275
			5.0	3.0	0.904	0.222
			10.0	3.1	1.569	0.299
9	4	95.957	1.0	3.5	0.384	0.171
			5.0	2.8	0.295	0.119
			10.0	2.2	0.304	0.095
3	16	96.593	0.5	5.9	5.687	1.085
			1.0	5.2	4.757	0.873
			2.5	4.1	2.429	0.494
			5.0	3.4	2.542	0.414
			10.0	3.5	3.194	0.335
3	27	128.451	1.0	5.8	9.300	1.339
			2.5	5.1	6.864	1.014
			5.0	4.6	4.520	0.748
			10.0	3.9	4.683	0.635
9	16	141.996	0.1	8.0	8.039	1.261
			0.5	6.1	5.494	0.782
			1.0	5.4	4.490	0.625
			2.5	4.8	3.619	0.499
			5.0	4.7	2.845	0.435
			10.0	3.7	2.666	0.328

TABLE 2: Summary of the Trajectory Calculations for OH(v',j'=1) + O_2(v'',j''=1) → O_3 + H

v'	v''	$E_{vib/rot}$, kcal mol^{-1}	E_{tr}, kcal mol^{-1}	b_{max}, Å	σ^{O3}, Å^2	$\Delta\sigma^{O3}$, Å^2
9	4	95.957	5.0	1.8	0.143	0.053
			10.0	1.8	0.305	0.078
3	16	96.593	10.0	0.7	0.018	0.007
3	27	128.451	1.0	5.8	6.975	1.173
			2.5	4.5	3.563	0.654
			5.0	4.3	4.299	0.680
			10.0	3.9	2.580	0.483
9	13	131.478	0.5	6.3	26.933	2.295
			1.0	5.3	16.943	1.554
			2.5	4.7	10.549	1.114
			5.0	4.1	8.766	0.878
			10.0	3.8	6.714	0.720
9	16	141.996	0.1	8.1	50.705	2.810
			0.5	6.4	31.913	1.757
			1.0	5.7	22.762	1.344
			2.5	5.1	15.525	1.014
			5.0	4.7	13.394	0.866
			10.0	4.1	9.136	0.632
9	27	173.854	1.0	6.1	52.838	2.602
			2.5	5.8	40.582	2.299
			5.0	5.5	29.650	1.969
			10.0	5.0	20.106	1.533

TABLE 3: Summary of the Trajectory Calculations for OH(v'=0,j'=10) + O_2(v''=27,j''=1) → HO_2 + O

E_{tr}, kcal mol^{-1}	b_{max}, Å	σ^{HO_2}, Å^2	$\Delta\sigma^{HO_2}$, Å^2
0.5	6.2	7.246	1.283
1.0	5.6	5.517	1.013
5.0	3.9	3.536	0.559
10.0	3.6	4.031	0.385
15.0	3.6	4.845	0.417
20.0	3.3	4.413	0.362

Batches of up to 2000 trajectories have then been carried out for each translational energy and vibrational−rotational combination.

For a given value of the translational energy, the specific reactive cross section for formation of product x assumes the form

TABLE 4: Summary of the Trajectory Calculations for OH(v'=0,j'=10) + O_2(v''=27,j'') → O_3 + H

j''	$E_{vib/rot}$, kcal mol^{-1}	E_{tr}, kcal mol^{-1}	b_{max}, Å	σ^{O_3}, Å^2	$\Delta\sigma^{O_3}$, Å^2
1	104.761	10.0	1.5	0.057	0.020
		15.0	1.9	0.170	0.044
		20.0	1.7	0.369	0.052
9	104.996	10.0	1.2	0.063	0.024
		15.0	1.9	0.159	0.060
		20.0	1.7	0.254	0.067

$$\sigma^{x}_{v'j',v''j''} = \pi b_{max}{}^2 P^{x}_{v'j',v''j''} \tag{10}$$

with the associated 68% uncertainaties being given by

$$\Delta\sigma^{x}_{v'j',v''j''} = \left(\frac{N_{v'j',v''j''} - N^{x}_{v'j',v''j''}}{N_{v'j',v''j''}N^{x}_{v'j',v''j''}}\right)^{1/2} \sigma^{x}_{v'j',v''j''} \tag{11}$$

where $N^{x}_{v'j',v''j''}$ denotes the number of reactive trajectories yielding product x in a total of $N_{v'j',v''j''}$ for the combination ($v'j'$,$v''j''$) of the colliding molecules, and $P^{x}_{v'j',v''j''}$ is the corresponding reactive probability. From the reactive cross section and assuming a Maxwell−Boltzmann distribution over the translational energy (E_{tr}), the specific thermal rate coefficient is obtained as

$$k^{x}_{v'j',v''j''}(T) = g_e(T)\left(\frac{2}{k_B T}\right)^{3/2}\left(\frac{1}{\pi\mu}\right)^{1/2}\int E_{tr}\sigma^{x}_{v'j',v''j''}\exp\left(-\frac{E_{tr}}{k_B T}\right)\mathrm{d}E_{tr} \tag{12}$$

where $g_e(T) = {}^1/_3[1 + \exp(-205/T)]^{-1}$ is the appropriate electronic degeneracy factor, k_B is the Boltzmann constant, μ is the reduced mass of the colliding diatomic particles, and T is the temperature.

4. Results and Discussion

Tables 1− 4 summarize the trajectory calculations carried out for the OH(v',j') + O_2(v'',j'') reaction. Note that in paper I we have done the analysis of the different channels leading to HO_2 formation. The difference now is that, for highly vibrationally excited OH, the probability of breaking this bond increases and the fraction of HO_2 molecules formed via such a route becomes of the same order of magnitude as for the oxygen-atom abstraction mechanism (see eq 10 to eq 12 of ref 33). No formation of ozone has been found for the combinations OH(v'=9,j'=1) + O_2(v''=2,j''=1) and OH(v'=3,j'=1) + O_2(v''=13,j''=1). For internal energies close to 96 kcal mol^{-1}, the cross section for ozone formation is found to be small (one or 2 orders of magnitude smaller than that for HO_2 at corresponding internal and translational energies). Of course, both channels get closed for combinations below the associated endoergicity if zero-point energy leakage is ignored (see later).

4.1. Dynamical Features. The dependences of the maximum impact parameter with translational energy for formation of HO_2 (a) and O_3 (b) is shown in Figure 3. As expected, the maximum impact parameter increases with internal energy of the reactants for a fixed translational energy. It is seen that reaction may occur both via capture-type and barrier-type mechanisms. For low internal energies, OH(v'=0,j'=1,10) and O_2(v''=13,j''=1,9), HO_2 formation dominates (as expected since the total available energy is below the threshold for O_3 formation), and one encounters a regime typical of a reaction with a threshold energy. This is so for all studied translational energies [see paper I for the case OH(v'=0,j'=1) and O_2(v''=13,j''=1)]. For high internal energy values, b_{max} is found to increase with decreasing

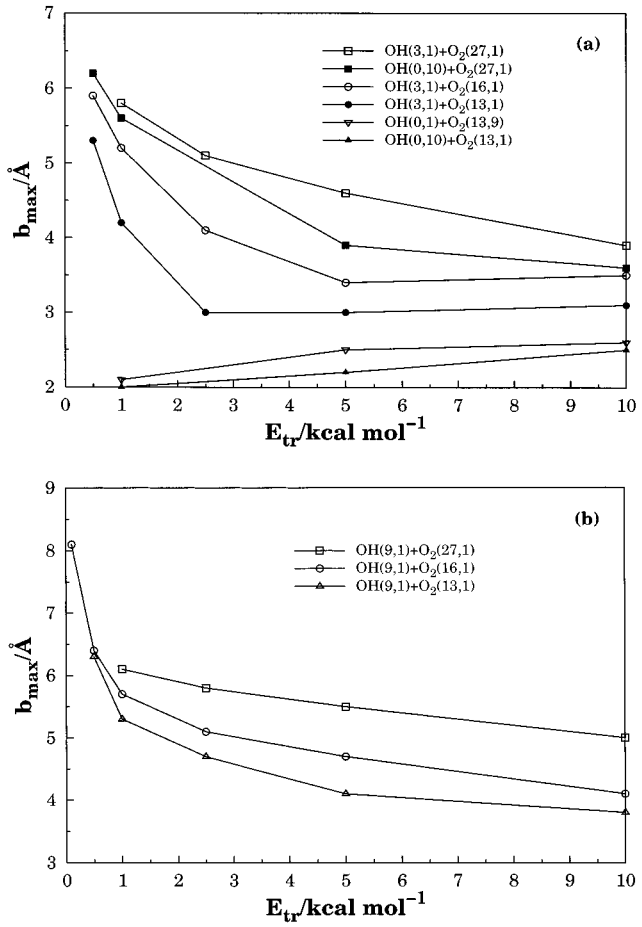

Figure 3. Energy dependence of the maximum impact parameter for some vibrorotational combinations of the reactant molecules: (a) HO_2 + O and (b) O_3 + H formation.

translational energy, as it usually happens in reactions occurring via a capture-type mechanism. However, for high translational energies (the transition between the two regimes occurs for an internal energy of about 70 kcal mol^{-1}), b_{max} is essentially constant or even slightly increases with E_{tr}. When the internal energy of reactants is very high [OH(v'=9,j' =1) and O_2-(v''=13,16,27,j''=1)], ozone production dominates (see Table 1 and Table 2) and one expects it to be dictated by a capture-type mechanism. The above dependences of b_{max} on E_{tr} and internal energy of reactants may be rationalized by noting that the dominant interaction between OH and O_2 is, at large distances, of the dipole−quadrupole electrostatic type. In fact, the reactants are vibrationally excited (such a stretching leads to an increase of its dipole and quadrupole moments over the range of the excitations considered in present work), and hence one expects the attractive long-range forces to increase for the most favorable approaching orientations. Together with the enlarged molecular size, such an increase of the long-range forces may explain the ordering encountered for the various curves.

Figure 4 shows a typical opacity function for formation of O_3. Note that the abcissae in these plots are b/b_{max}, with b_{max} being the largest impact parameter found in the present work (8.1 Å). The notable feature from this figure is perhaps the fact that the opacity function shows only one pattern: it increases with impact parameter showing the effect of long-range forces. For formation of HO_2, opacity functions similar to those reported in paper I for barrier-type and capture-type regimes were obtained.

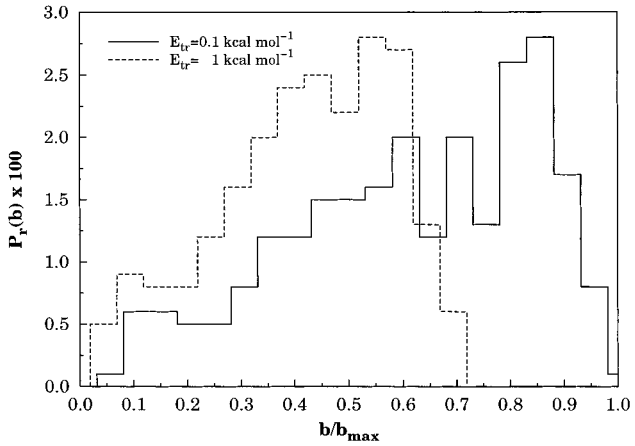

Figure 4. Opacity function of O_3 in the reaction OH(v'=9,j'=1) + O_2(v''=16,j''=1).

TABLE 5: Average Values of Complex Lifetime (in All Cases j'' = 1)

			E_{tr}/kcal mol^{-1}		
(v',j')	v''	product	1.0	5.0	10.0
(9,1)	4	HO_2		0.229	0.119
(3,1)	13		0.195	0.187	0.157
(0,10)	27			0.155	0.085
(3,1)	27		0.224	0.098	0.084
(3,1)	27	O_3	0.113	0.095	0.083
(9,1)	16		0.052	0.059	0.056

Using the model developed in paper I, we have estimated the average lifetime of the HO_3 complex for different initial translational energies corresponding to barrier-type and capture-type regimes. Some of these values are reported in Table 5 as obtained from all reactive trajectories referring to such batches. In the case of HO_2 formation, the average lifetime of the complex for a given initial vibrational−rotational combination is found as expected to decrease with increasing translational energy. However, for a fixed translational energy and internal state of OH, such a lifetime decreases with increasing internal energy of the O_2 molecule. This result may be explained by recalling that the majority of HO_2 radicals are produced by breaking the O_2 bond, an event more likely to occur when the O_2 molecule is vibrationally excited. A corresponding analysis may be done for the case of O_3 formation by considering now the excitation of OH. For highly excited OH radicals, such a lifetime is virtually independent of the translational energy and shorter than for HO_2 formation, which may be indicative of rupture of the OH bond. For low values of internal energy of OH, formation of HO_2 tends to proceed via breaking the O_2 molecule. However, when the OH molecule is highly vibrationally excited, the possibility of rupture of the OH radical followed by capture of the H atom by the unbroken O_2 molecule becomes significant.

4.2. Energetic Features. The partitioning of energy release in the product molecules is calculated from the output values produced by the MERCURY/VENUS96[40] codes and is shown in Table 6 for some initial combinations. Clearly, the outcoming molecules have a considerable internal energy content, with a significant part of it being in the rotational degrees of freedom, i.e., part of the energy of the system has been converted into rotational energy of the products. In fact, a significant fraction of the product O_3 molecules has a vibrational energy above the O_2 + O dissociation threshold which is 25.37 kcal mol^{-1}. This result shows an interesting similarity with the findings reported elsewhere[26,28] for the $O_2(v)$ + $O_2(v)$ reaction and implies that

TABLE 6: Energy Distribution among the Diferent Degrees of Freedom

(v',j')	(v'',j'')	E_{tr}, kcal mol^{-1}	$\langle E_{tr}\rangle$, kcal mol^{-1}	%	$\langle E_{vib}\rangle$, kcal mol^{-1}	%	$\langle E_{rot}\rangle$, kcal mol^{-1}	%
				HO_2				
(3,1)	(13,1)	1.0	5.4	14.6	24.6	66.3	7.1	19.1
		5.0	8.1	19.9	28.0	68.8	4.6	11.3
		10.0	7.6	16.7	30.7	67.6	7.1	15.7
(0,10)	(27,1)	1.0	9.0	16.5	37.4	68.6	8.1	14.9
		5.0	11.3	19.2	34.8	59.0	12.9	21.8
		10.0	14.5	22.6	36.6	57.0	13.1	20.4
				O_3				
(9,1)	(13,1)	1.0	13.8	26.2	35.5	67.2	3.5	6.6
		5.0	12.3	21.5	38.6	67.5	6.3	11.0
		10.0	14.0	22.5	40.1	64.6	8.0	12.9
				OH + O_2[a]				
(3,1)	(13,1)	1.0			23/36[b]		7/5[c]	
		5.0			24/37		7/6	
		10.0			25/39		7/6	
(0,10)	(27,1)	1.0			12/60		14/5	
		5.0			13/57		17/5	
		10.0			13/58		15/8	

[a] Nonreactive trajectories. [b] The two numbers on this column are related with the vibrational energy of the OH and O_2 molecules, respectively. [c] As in *a* but for rotational energy.

such vibrationally hot ozone ($O_3^\star$) molecules will dissociate once given enough time to do so. Thus, such trajectories might also be counted as forming O_2 + O + H. Since this has no implications on the conclusions to be drawn later, we will count as ozone forming trajectories those leading to both O_3 and $O_3^\star$. Indeed, any dissociating $O_3^\star$ species will finally lead again to a stable ozone molecule through three-body recombination of the outcoming oxygen atom with molecular oxygen.

We further observe from Table 6 that the average value of energy per degree of freedom in the products increases with increasing initial internal energy of the reactants, although the partitioning of the energy is qualitatively similar for all translational energies and combination of quantum numbers. Thus, the fraction or percent corresponding to each degree of freedom is on average practically independent of the initial energy conditions. This might suggest that reaction proceedes with formation of a complex. However, for direct reactions one might expect from Polanyi's rules (the saddle point occurs late in the products valley) that vibrational energy in the reactants would favor reaction and be converted into translational energy in the products. The fact that this last issue is not clearly visible from the present results may point out that such rules should be viewed with some caution when applied to reactions involving more than three atoms and having competitive channels. We emphasize the small dependence of the average values of energy per degree of freedom with translational energy, which has been rationalized in paper I. We can now add that the average energy partition for different degrees of freedom is essentially a function of the structural constants of the systems (mass, force constants, rotational constants, etc.). This may explain why it remains similar for a given product molecule and changes when one passes from HO_2 to O_3, especially when considering the products rotational energy.

Table 6 shows also the vibrational and rotational energies of the products for some batches of nonreactive trajectories. It is clear that both molecules (OH and O_2) retain a high level of internal excitation after the collisional event. Thus, the problem of zero-point energy leakage can be ignored for practical purposes, for both reactive (which are highly exoergic) and nonreactive events. In fact, the study of vibrational and rotational relaxation in V−T, V−R, and V−V collision processes is in itself an interesting topic, which will be left for a future publication.

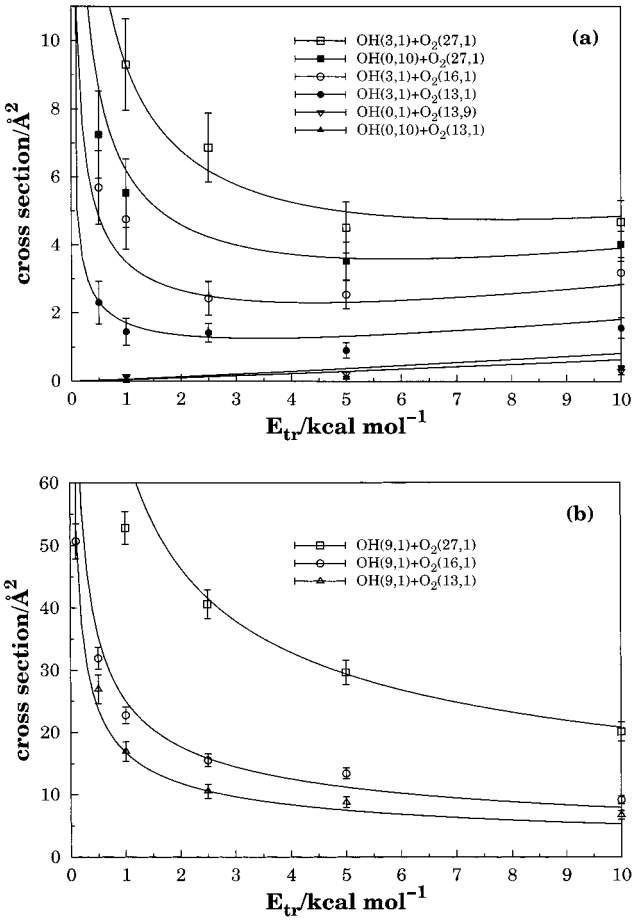

Figure 5. Reactive cross section σ^x as a function of the translational energy for HO_2 (a) and O_3 (b) formation. Also indicated are the 68% error bars and the fitted lines given by eqs 13 and 18.

4.3. Reactive Cross Sections. The studied reactions dominate for different combinations of initial quantum numbers. We find that HO_2 is the major product for internal energies below 128

kcal mol^{-1} [corresponding to the combination OH(v'=3,j'=1) + O_2(v''=27,j'=1)] while ozone becomes the dominant product for higher internal energies.

We now examine the shape of the excitation functions (cross section vs translational energy), which are shown in Figure 5 together with the associated 68% error bars for formation of HO_2 + O (Figure 5a) and O_3 + H (Figure 5b). The curves for formation of HO_2 have, in general, two opposite trends that explain their shapes. For low internal energies, OH(v'=0,j'=1,10) + O_2(v''=13,j''=1,9), the shapes of these curves correspond to a barrier-type behavior for the whole range of translational energies. Instead, for high internal energy values, the capture-type regime dominates at low translational energies, leading to the well established (e.g., refs 41 and 42 and references therein) decreasing dependence of the reactive cross section with E_{tr}. On the other hand, for high translational energies, one observes the common pattern found in reactions that have an energy threshold; i.e., $\sigma^{HO_2}_{v'j',v''j''}$ is an increasing function of E_{tr}. As a result, the excitation function shows a minimum in the region where the above two effects balance each other. In general $\sigma^{HO_2}_{v'j',v''j''}$ increases with internal energy at a fixed translational energy for internal energies below the combination OH(v'=3,j'=1) + O_2(v''=27,j''=1). For this combination, despite the reactive cross section of HO_2 being still larger than that corresponding to ozone formation, it reaches the same order of magnitude of the first, with competition making the values of $\sigma^{HO_2}_{v'j',v''j''}$ fall off. Clearly, curves for OH(v'=3,j'=1) + O_2(v''=13,j''=1) and OH(v'=3,j'=1) + O_2(v''=16,j''=1) with internal energies below the combination OH(v'=0, j'=1) + O_2(v''=27,j''=1) have a similar or even larger value of the reactive cross section, indicating the effectiveness of the vibrational energy in the OH molecule to enhance HO_2 formation (see paper I). This result may be explained by considering two features: first, an increase of OH stretching leads to a larger dipole moment; second, such a stretching increases naturally the probability of HO_2 formation via rupture of the OH bond.

The curves in Figure 5b show the reactive cross section for ozone formation when this is the major outcome. The notable feature is the fact that it shows only a capture-type regime over the studied range of translational energies, which is due to the high internal energies obtained from the vibrational energy of the OH molecule. These results lead to the conclusion that the OH vibrational energy effectively promotes rupture of the OH bond, while enhancing the role of long-range forces in ozone formation. It is interesting to note the high values obtained for the reactive cross section of ozone formation which substantially overpasses the values of the HO_2 reactive cross section for a given translational energy.

Tables 3 and 4 (see also Table 2 of paper I for $j' = 1$) show that the effect of the rotational degrees of freedom is essentially an energetic one, with the rotation of OH having a greater influence in HO_2 formation than the rotation of O_2. This is simply due to the higher value of the rotational quantum in OH. In relation to the ozone formation, such an influence is not significant due to the high levels of internal energy required to make relevant formation of the O_3 product. The curves in Figure 5 show the present calculations for several combinations including rotational quantum numbers $j' = 10$ and $j'' = 9$, which correspond to the optimum populations.[25,36]

To analytically describe the dependence of the cross section on translational energy, we have kept the form introduced in paper I to study HO_2 formation. Thus,

$$\sigma^{HO_2}(E_{OH},E_{O_2},E_{tr}) = \frac{f(E_{OH},E_{O_2})}{E_{tr}^{1/2}} + g(E_{OH},E_{O_2})E_{tr}^{6/5}\exp(-mE_{tr}) \quad (13)$$

where E_{OH} and E_{O_2} are the internal energies. To describe the effect of internal energy we have now introduced the functions

$$f(E_{OH},E_{O_2}) = (a_0 + a_1x^3)e^{-nx} \quad (14)$$

$$g(E_{OH},E_{O_2}) = (b_0 + b_1y^3)e^{-py} \quad (15)$$

where

$$x = \frac{E_{OH} + \xi_1E_{O_2} - E_{th}}{E_{th}} \quad (16)$$

$$y = \frac{E_{OH} + E_{O_2} - E'_{th}}{E'_{th}} \quad (17)$$

For ozone formation, the function has only the capture term leading to

$$\sigma^{O_3}(E_{OH},E_{O_2},E_{tr}) = \frac{f_1(E_{OH},E_{O_2})}{E_{tr}^{1/2}} \quad (18)$$

with

$$f_1(E_{OH},E_{O_2}) = (c_0 + c_1z + c_2z^2) \quad (19)$$

and

$$z = \frac{\xi_2E_{OH} + E_{O_2} - E''_{th}}{E''_{th}} \quad (20)$$

The parameters E_{th}, E'_{th}, and E''_{th} in eqs 16, 17, and 20 are energy threshold values of the corresponding arguments for the different processes (formation of HO_2 in the capture and barrier-type regimes and formation of O_3, respectively). In turn, ξ_1 and ξ_2 are parameters that help express the higher effectiveness of the internal energy of the OH molecule to promote ozone formation and the preferential effect of the internal energy of the oxygen molecule to form HO_2 due to the enhancement of O_2 breaking and increase of the quadrupole moment. The numerical values of all parameters are reported in Table 7. The exponential functions in eqs 14 and 15 account for the falloff due to the competition of other reactive channels. The remaining coefficients in eqs 14, 15, and 19 have been determined from a least-squares fitting procedure; their optimum numerical values are also reported in Table 7. The resulting fitted functions are shown together with the calculated points in Figure 5. It is seen that the model reflects the general trends of the calculations. Note that the representation depends only on the internal energy of the reactants species, but not on any specific model that expresses the dependence of the internal energy with the quantum numbers. The use of the same dependence with translational energy introduced in paper I for the HO_2 product led to the same functional form as a function of temperature. Thus, we may write from eq 13,

TABLE 7: Numerical Values[a] for Coefficients of the Cross Section Functions

E_{th}	73	E'_{th}	57	E''_{th}	130
χ_1	1.3	χ_2	1.5	m	0.008
a_0	0.34717	a_1	43.65244	b_0	0.05580
b_1	2.54724	c_0	6.09767	c_1	−5.69639
c_2	139.01760	n	1.73498	p	2.89917

[a] The units are such that cross section is Å^2 and energy is kcal mol^{-1}.

$$k^{HO_2}(E_{OH},E_{O_2},T) = g_e(T)\left(\frac{8}{\pi\mu}\right)^{1/2}\left[\Gamma(^3/_2)f(E_{OH},E_{O_2}) + \Gamma(16/5)g(E_{OH},E_{O_2})\left(\frac{(k_BT)^{17/10}}{(1+mk_BT)^{16/5}}\right)\right] \quad (21)$$

From the previous equation it is easy to show that the temperature dependence of k^{HO_2} is essentially determined by the electronic degeneracy factor $g_e(T)$. In the range of small temperatures that are of interest in atmospheric chemistry (these are determined by the condition $k_BT \ll m^{-1}$), eq 21 can be approximately expressed as

$$k^{HO_2}(E_{OH},E_{O_2},T) = g_e(T)\left(\frac{8}{\pi\mu}\right)^{1/2}[\Gamma(^3/_2)f(E_{OH},E_{O_2}) + \Gamma(16/5)g(E_{OH},E_{O_2})(k_BT)^{17/10}] \quad (22)$$

A comparison of eqs 13 and 22 with the corresponding ones in paper I leads to the conclusion that the form of the temperature dependence is approximately the same but scaled by the functions which express the influence of internal energy. Thus, eq 21 leads to substantially higher values of the specific rate coefficient for formation of the hydroperoxyl radical than in paper I. For the ozone formation, we obtain

$$k^{O_3}(E_{OH},E_{O_2},T) = g_e(T)\left(\frac{8}{\pi\mu}\right)^{1/2}\Gamma(^3/_2)f_1(E_{OH},E_{O_2}) \quad (23)$$

Figure 6 shows the curves in eq 21 and eq 23 for several internal energies. For completeness, we show in Figure 7 thecalculated vibrationally averaged thermal rate coefficients for both reactions as given by

$$k^X(T) = \frac{\Sigma_{v'=v'_0{}^X}\Sigma_{v''=v''_0} w_{v'}w_{v''}k^X(E_{OH}(v',j'=10),E_{O_2}(v'',j''=1))}{\Sigma_{v'=0}\Sigma_{v''=0}w_{v'}w_{v''}} \quad (24)$$

where $v'^{HO_2}_0 = 0$; $v'^{O_3}_0 = 7$, and $v''_0 = 13$. The vibrational populations $w_{v''}$ of oxygen are those obtained in the 226 nm photolysis of ozone,[24] while the OH vibrational populations $w_{v'}$ are taken from the experimental work of Ohoyama et al.[18] As Figure 7 shows, the vibrationally averaged thermal rate coefficient for O_3 formation decreases with temperature from about 7×10^{-11} cm^3 molecule^{-1} s^{-1} at ultralow temperatures to about 4.5×10^{-11} cm^3 molecule^{-1} s^{-1} at $T = 500$ K. Moreover, it is found to be about 5 times larger than the corresponding calculated rate for HO_2 formation and of the order of magnitude of the rate suggested[24,26] for the process $O_2(v=0) + O_2(v=27) \rightarrow O_3 + O$. Thus, it should not be overlooked when discussing the so-called "ozone deficit" problem, which we have addressed in the Introduction.

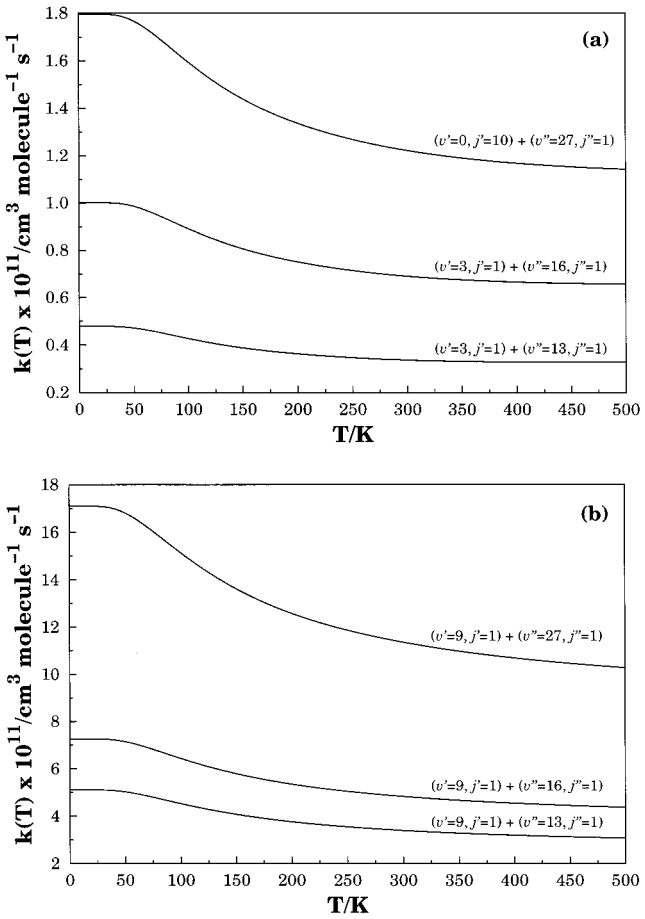

Figure 6. Specific thermal rate coeficients for the title reaction for (a) HO_2 and (b) O_3 formation.

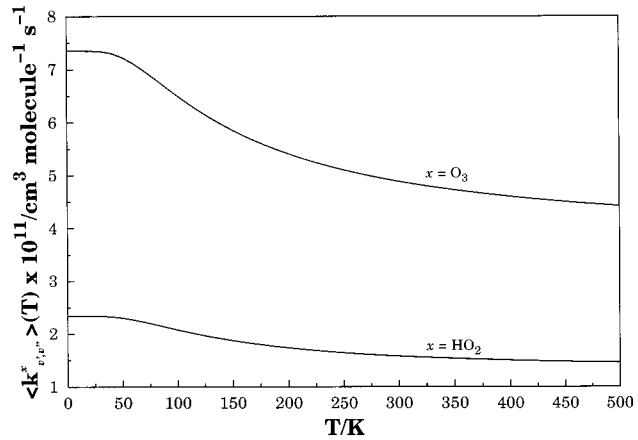

Figure 7. Vibrationally averaged thermal rate coefficient for the title reactions.

5. Conclusions

We have carried out a QCT study of the branching reaction $OH(v',j') + O_2(v'',j'')$ for several combinations of rotational and vibrational quantum numbers. The calculations have shown two distinct regimes as a function of the reactants internal energy. For low initial internal energies of the reactant species, hydroperoxyl formation is dominant over the whole range of translational energies. This applies to the combination $OH(v'=0,j'=1) + O_2(v''=13,j''=1)$ and larger v'' values. For high internal energies, ozone formation is predicted to be the major process in our calculations [$OH(v'=9,j'=1) + O_2(v''=13,16,27,j''=1)$], with very large values being obtained for the corresponding reactive cross section in comparison with those for HO_2 formation. The calculations also suggest that rotational excitation has essentially an energetic role. Thus,

rotation of OH (which has a larger rotational quantum than O_2), leads to a significant increase in the HO_2 reactive cross section while rotational excitation of O_2 has only a small effect. Conversely, for ozone formation, rotational excitation is not relevant (at least in the region where this product is dominant). No comparison with experimental data has been possible due to the unavailability of such data. The results from the present work also suggest that the products of the title branching reaction can be controlled by vibrational stimulation of the proper reactant molecule: vibrational excitation of O_2 enhances hydroperoxyl formation, while vibrational excitation of OH enhances ozone formation. We hope that the present study may stimulate works using laser techniques, which allow the preparation of vibrationally hot reactant molecules. Finally, we note that the studied products have a very low reactive cross section in normal conditions due to having a high endoergicity. However, one may speculate that existing nonequilibrium conditions in the stratosphere make them relevant for the study of atmospheric chemistry. This fact may be more dramatic in the case of ozone, for which the rate coefficient has been shown to have a more drastic variation with the initial internal energy combination.

Acknowledgment. This work has the support of Fundação para a Ciência e Tecnologia, Portugal, under the program PRAXIS XXI. Some of the calculations have been carried out with the financial support to J.D.G. of the German Academic Exchange Service (DAAD) and the Third World Academy of Sciences (TWAS Research Grant No. 97-144, RG/CHE/LA).

References and Notes

(1) Wayne, R. P. *Chemistry of Atmospheres*; Clarendon: Oxford, U.K., 1991.
(2) Varandas, A. J. C. *Int. Rev. Phys. Chem.* **2000**, *19*, 199.
(3) McDade, J. C.; Llewellyn, E. *J. Geophys. Res.* **1987**, *92*, 7643.
(4) Crutzen, P. *Science* **1997**, *277*, 1951.
(5) Summers, M. E.; Conway, R. R.; Siskind, D. E.; Stevens, M. H.; Offermann, D.; Riese, M.; Preusse, P.; Strobel, D. F.; Russell, J. M., III. *Science* **1997**, *277*, 1967.
(6) Anlauf, K. G.; Macdonald, R. G.; Polani, J. C. *Chem. Phys. Lett.* **1968**, *1*, 619.
(7) Polanyi, J. C.; Sloan, J. J. *Int. J. Chem. Kinet. Symp.* **1975**, *1*, 51.
(8) Keyser, L. F. *J. Phys. Chem.* **1979**, *83*, 645.
(9) Clyne, M. A. A.; Monkhouse, P. B. *J. Chem. Soc., Faraday Trans. 2* **1977**, *73*, 298.
(10) Phillips, L. F.; Schiff, H. I. *J. Chem. Phys.* **1962**, *37*, 1233.
(11) Lee, J. H.; Michael, J. V.; Payne, W. A.; Stief, L. J. *J. Chem. Phys*. **1978**, *69*, 350.
(12) Greenblatt, G. D.; Wiesenfeld, J. R. *J. Geophys. Res.* **1982**, *87*, 11145.
(13) Finlayson-Pitts, B. J.; Kleindienst, T. E.; Ezell, M. J.; Toohey, D. W. *J. Chem. Phys.* **1981**, *74*, 4533.
(14) Washida, N.; Akimoto, H.; Okuda, M. *J. Chem. Phys.* **1980**, *72*, 5781.
(15) Finlayson-Pitts, B. J.; Kleindienst, T. E. *J. Chem. Phys.* **1979**, *70*, 4804.
(16) Howard, C. J.; Finlayson, B. J. *J. Chem. Phys.* **1980**, *72*, 3842.
(17) Force, A. P.; Wiesenfeld, J. R. *J. Chem. Phys.* **1981**, *74*, 1718.
(18) Ohoyama, H.; Kasai, T.; Yoshimura, Y.; Kuwata, H. *Chem. Phys. Lett.* **1985**, *118*, 263.
(19) Zhurt, C.; Zülicke, L.; Umansky, S. Y. *Chem. Phys.* **1986**, *105*, 15.
(20) Zhurt, C.; Zülicke, L. *Chem. Phys. Lett.* **1984**, *111*, 408.
(21) Shalashilin, D. V.; Umanskii, S. Y.; Gershenzon, Y. M. *Chem. Phys.* **1992**, *168*, 315.
(22) Dodd, J. A.; Lipson, S. J.; Blumberg, W. A. M. *J. Chem. Phys.* **1991**, *95*, 5752.
(23) Shalashilin, D. V.; Michtchenko, A. V.; Umanskii, S.; Gershenzo, Y. M. *J. Phys. Chem.* **1995**, *99*, 11627.
(24) Miller, R. L.; Shuits, A. G.; Houston, P. L.; Toumi, R.; Mack, J. A.; Wodtke, A. M. *Science* **1994**, *265*, 1831.
(25) Wang, W.; González-Jonte, R.; Varandas, A. J. C. *J. Phys. Chem. A* **1998**, *102*, 6935.
(26) Varandas, A. J. C.; Wang, W. *Chem. Phys.* **1997**, *215*, 167.
(27) Price, J. M.; Mack, J. A.; Rogaski, C. A.; Wodtke, A. M. *Chem. Phys.* **1993**, *175*, 83.
(28) Wang, W.; Varandas, A. J. C. *Chem. Phys*. **1998**, *236*, 181.
(29) Varandas, A. J. C.; Pais, A. A. C. C.; Marques, J. M. C.; Wang, W. *Chem. Phys. Lett.* **1996**, *249*, 264.
(30) Rogaski, C. A.; Price, J. M.; Mack, J. A.; Wodtke, A. M. *Geophys. Res. Lett.* **1993**, *20*, 2885.
(31) Toumi, R.; Houston, P. L.; Wodtke, A. M. *J. Chem. Phys.* **1996**, *104*, 775.
(32) Geiser, J.; Dylewski, S. M.; Mueller, J. A.; Willson, R. J.; Toumi, R.; Houston, P. L. *J. Chem. Phys.* **2000**, *112*, 1279.
(33) Garrido, J. D.; Caridade, P. J. S. B.; Varandas, A. J. C. *J. Phys. Chem. A* **1999**, *103*, 4815.
(34) Varandas, A. J. C.; Yu, H. G. *Mol. Phys*. **1997**, *91*, 301.
(35) Varandas, A. J. C.; Szichman, H. *Chem. Phys. Lett.* **1998**, *295*, 113.
(36) Yu, H. G.; Varandas, A. J. C. *J. Chem. Soc., Faraday Trans.* **1997**, *93*, 2651.
(37) Szichman, H.; Baer, M.; Varandas, A. J. C. *J. Phys. Chem. A* **1997**, *101*, 8817.
(38) Yu, H. G.; Varandas, A. J. C. *Chem. Phys. Lett.* **2001**, *334*, 173.
(39) Varandas, A. J. C.; Caridade, P. J. S. B. *Chem. Phys. Lett.*, in press.
(40) Hase, W. L. MERCURY: a general Monte Carlo classical trajectory computer program, QCPE#453. An updated version of this code is VENUS96: Hase, W. L.; Duchovic, R. J.; Hu, X.; Komornik, A.; Lim, K. F.; Lu, D.-H.; Peslherbe, G. H.; Swamy, K. N.; van de Linde, S. R.; Varandas, A. J. C.; Wang, H.; Wolf, R. J. *QCPE Bull.* **1996**, *16*, 43.
(41) Smith, I. W. *Kinetics and Dynamics of Elementary Gas Reactions*; Butterworkth: Boston, 1980.
(42) Levine, R. D.; Bernstein, R. B. *Molecular Reaction Dynamics and Chemical Reactivity*; Oxford University Press: New York, 1987.